N70 41377

1706

TR-1

CR 113951

NATIONAL AERONAUTICS AND SPACE ADMINISTRATION
LUNAR SAMPLE ANALYSIS PROGRAM

PREPARATION FOR AN INVESTIGATION OF THE THERMAL RADIATION CHARACTERISTICS AND THERMAL CONDUCTIVITY OF LUNAR MATERIAL

Final Report for 1968

PREPARATION FOR LUNAR MATERIAL THERMOPHYSICAL PROPERTY MEASUREMENTS

by

Richard C. Birkebak

and

Clifford J. Cremers

CASE FILE COPY

February 1969

Principal Investigator: Richard C. Birkebak

Co-Investigators: Clifford J. Cremers
and James P. Dawson
Lunar Receiving Laboratory
Manned Spacecraft Center

Prepared under Grant No. NGR 18-001-026

by

HIGH TEMPERATURE AND THERMAL RADIATION LABORATORY
Department of Mechanical Engineering
University of Kentucky
Lexington, Kentucky

NATIONAL AERONAUTICS AND SPACE ADMINISTRATION
Washington, D. C.

CONTENTS

	Page
Abstract	i
Summary	ii
Introduction	1
Part I Vacuum System Design	1
Part II Thermal Radiation Studies	3
Part III Thermal Conductivity Measurements	22

ILLUSTRATIONS

	Illustrations
Vacuum System - photograph	I-1
Vacuum Manifold System	I-2
Vacuum Manifold Subsystem	I-3
Vacuum Manifold Subsystem	I-4
Irradiance on the Sphere Wall with plane MgO/MgO Samples	II-1
Irradiance on the Sphere Wall Using A Computer Technique	II-2
Sample Blockage Effects Due to Sample Displacement	II-3
Coordinate System	II-4
Schematic View of Guarded Plate Apparatus	III-1
Data from Typical Line Heat Source Run	III-2
Schematic View of Large Line Heat Source Probe	III-3

Illustrations

Schematic View of Small Line Heat Source Cell III-4

Schematic View of Line Heat Source Probe III-5

PREPARATION FOR LUNAR MATERIAL THERMOPHYSICAL PROPERTY MEASUREMENTS

by

Richard C. Birkebak

and

Clifford J. Cremers

Abstract

This report describes work performed in the preparation of equipment and measurement techniques to be used on lunar material. An experimental study of the effects of sample size on the performance of the modified integrating sphere was carried out. The results indicate that the absolute reflectance can be obtained using the proposed displacement technique. Detailed studies of two techniques for the measurement of thermal conductivities were made and results obtained on a few simulated lunar materials.

Descriptors

General: Reflectometer, thermal conductivity,

Specific: Integrating sphere, line heat source, powders, reflectance,

PREPARATION FOR LUNAR MATERIAL THERMOPHYSICAL PROPERTY MEASUREMENTS

by

Richard C. Birkebak

and

Clifford J. Cremers

Associate Professors
Department of Mechanical Engineering
University of Kentucky

Summary

This final report describes work performed on National Aeronautics and Space Administration Research Grant NGR 18-001-026 for the period from July 1, 1967 to December 31, 1968. The work subdivides into three major areas: vacuum system and chamber design, thermal radiation studies, and thermal conductivity studies.

Vacuum System

A complete vacuum system including manifolds and four chambers was designed and ordered. The system has the capabilities of 260 liters/sec. at pressures to 10^{-9} torr. The four chambers were designed to match the requirements of the Lunar Receiving Laboratory (LRL). The chambers

are compatible with the sample handling system to be supplied by the LRL. Two of the chambers are spherical in shape and are to be used for visible and infrared directional reflectance measurement. A third was designed for directional emittance and bidirectional reflectance measurements while the fourth was designed for thermal conductivity measurements. These systems have been ordered and received by our laboratory.

Thermal Radiation Studies

The measurement of thermal radiation properties of powdered materials such as the lunar material may be, requires in some cases special handling techniques. For directional reflectance measurements the sample must remain fixed in a horizontal plane while the apparatus is rotated. Besides the above procedural problem for powdered material a further problem was encountered by the authors in preparing for lunar materials.

The amount of lunar sample available for measurement is contingent upon the amount returned to earth. In our case we must also make some compromises between thermal conductivity and thermal radiation measurements in regard to sample size and depth requirements. Because of these conditions an experimental program was carried out to determine several effects of sample size on integrating sphere performance and measurements.

The modified integrating sphere reflectometer has become a standard instrument for reflectance measurements. In the use of the modified integrating sphere a sample is placed at the center of the sphere and by rotating the sample the directional reflectance can be measured. The effects of a center-mounted sample on the sphere performance have been discussed by several authors. The introduction of a center-mounted sample affects the uniformity of the sphere wall irradiance even though the sphere wall and sample surfaces are perfectly diffuse reflectors.

The present work is an experimental study of the blockage effects of

a centrally located sample on the measurement of the absolute reflectance in the modified integrating sphere. The experiment was carried out for various sphere to sample radius ratios, and reflectances of front and back surface of the test sample.

The technique used to obtain absolute reflectance we refer to as the displacement method. In this method the sample is illuminated at the center of the integrating sphere and then the sample is displaced one diameter and the sphere wall illuminated. The ratio of a detector output for the sample to wall reading is the absolute reflectance. Our results indicate that for sample to sphere diameters from 0.06 to 0.2 that the above technique gives reflectance results within 1 percent of each other. Therefore, with the reflectometers as presently designed the amount of lunar material available is not critical to our measurements.

The experimentally measured wall irradiance is compared to a simple second order theory for wall irradiance distribution and agreement is found to be excellent.

Thermal Conductivity Studies

The proposed thermal conductivity measurements have not been carried out on simulated lunar material because of a delay in delivery of the infrared spectrometer. However, a high temperature test cell has been built for use in an existing vacuum chamber. It should be possible to check out the proposed method using this cell and a near infrared spectrometer.

Three test cells and one line heat source thermal conductivity probe have been built for making standard conductivity measurements of simulated material. These methods are being developed to provide a backup for the more novel method proposed. The measurements made with these cells on standard materials--glass beads and standard silicate rock samples--agree well with those from other investigations.

Introduction

This report describes the work performed on National Aeronautics and Space Administration Grant NGR 18-001-026 from July 1, 1967 to December 31, 1968 in the preparation of equipment and development of measurement techniques to be used on lunar material. During this reporting period three parallel efforts were undertaken: vacuum manifold and chamber designs; thermal radiation studies; and thermal conductivity studies. Each of these efforts are discussed under separate headings in this report.

There are several problems that arise when one considers the nature of lunar material and the measurement of its physical properties. If the lunar material is in powdered form the sample must remain fixed in a horizontal plane. In order to obtain meaningful test results on the thermal conductivity and thermal radiation characteristics the lunar material must also be kept under vacuum conditions. The amount of lunar sample available for measurements is contingent upon the amount returned to earth. In our case we must also make some compromises between thermal conductivity and thermal radiation measurements in regard to sample size and depth requirements. Because of these conditions, experimental programs were carried out to determine the amount of lunar material needed for both thermal conductivity and radiation studies.

Part I Vacuum System Design

An initial appraisal of the measurement techniques to be used to obtain the thermal radiation characteristics and thermal conductivity of lunar material, indicated that four vacuum chambers were required.

The measurement of the thermal radiation characteristics requires three chambers and the thermal conductivity method one chamber. These

include two vacuum integrating sphere systems; one each for the UV-visible region of the spectrum and one for the infrared region; a third chamber for directional emittance and bidirectional reflectance; and a fourth chamber for the thermal conductivity and hemispherical emittance studies. All of these systems are on order or received from Varian Associates at the present time.

Two vacuum integrating sphere systems, when complete, will allow us to measure the directional reflectance of the lunar material as a function of wavelength and angle of illumination. Each sphere is approximately eight inches in diameter with four ports, one each for the sample mounting, source, detecting system, and pumping.

The bidirectional reflectance and directional emittance chamber has been designed to have the capabilities of measuring these radiation characteristics as a function of angle of illumination and viewing. The chamber can be LN_2 cooled to eliminate any background radiation. Within this chamber will be a multiple yoke apparatus [goniometric device], for illuminating and viewing of the test sample.

The manifold system and test chambers for bidirectional reflectance and the thermal conductivity measurements received from Varian Associates are shown in Figure I-1. They have been constructed so as to be compatible with the 10^{-8} torr vacuum system being installed at present. The chambers have been provided with a number of strategically located access ports so as to provide maximum flexibility. A large access port has been provided at the top of the thermal conductivity chamber to allow the placement of LN_2 cooled shrouds about the test cell so as to provide an essentially non-radiating environment which is necessary for accurate measurement of the proposed measurement technique.

The four chambers are connected to a common manifold system, Figures I-2, I-3, and I-4, which is in turn connected to a Welch turbomolecular pump. The entire system to which the lunar material will be exposed is constructed from 304SS.

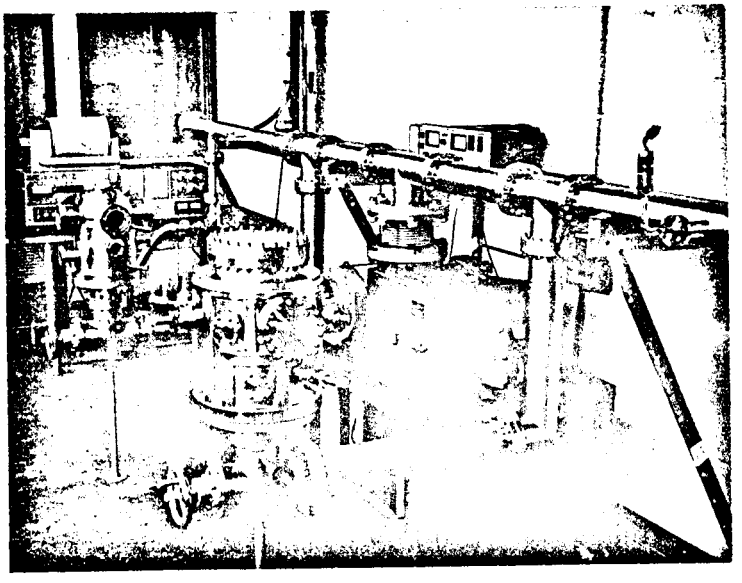

Figure I-1

VACUUM MANIFOLD SYSTEM

Delivery date 8 weeks after receipt of order.

System specifications; Pressures down to 10^{-9} torr. When blanked off, no leak detectable on a mass spectrometer leak detector with a sensitivity of 2×10^{-10} std cc/sec.
All surfaces exposed to vacuum should be stainless steel

Material: 4" O.D. 304 stainless steel, other dimensions as shown on drawing
Fittings: All valves and flanges to be VARIAN or equivalent.

Note; CFF Conflat flanges

Subsystem (1)

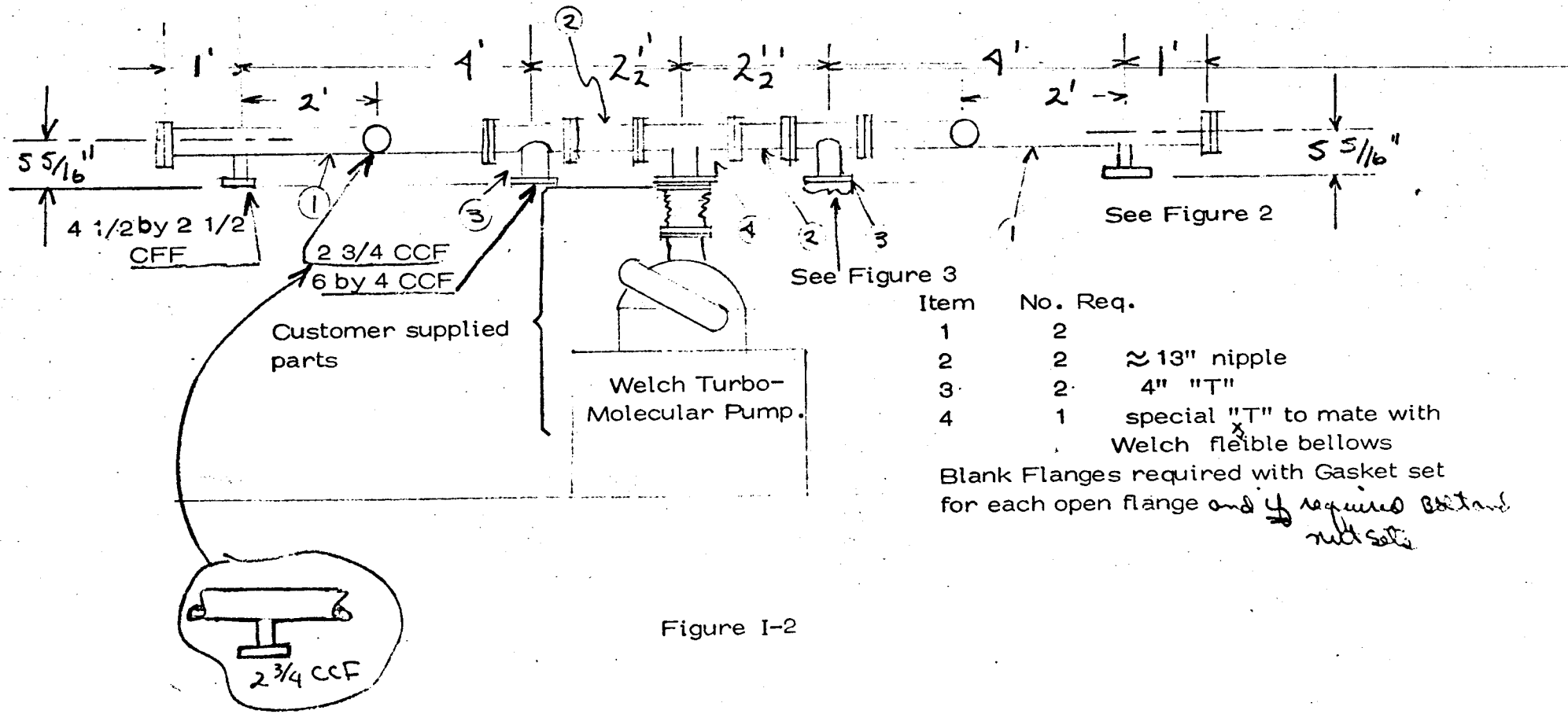

Item	No. Req.	
1	2	
2	2	≈ 13" nipple
3	2	4" "T"
4	1	special "T" to mate with Welch flexible bellows

Blank Flanges required with Gasket set for each open flange and if required Bolt and nut sets

Figure I-2

Subsystem (3)

TWO (2) Systems required. To match manifold system shown on Figure 1

Item	Description
1	4" O.D. stainless steel rt angle elbo as shown
2	24" nipple
3	4" rt angle Viton valve with back to air valve

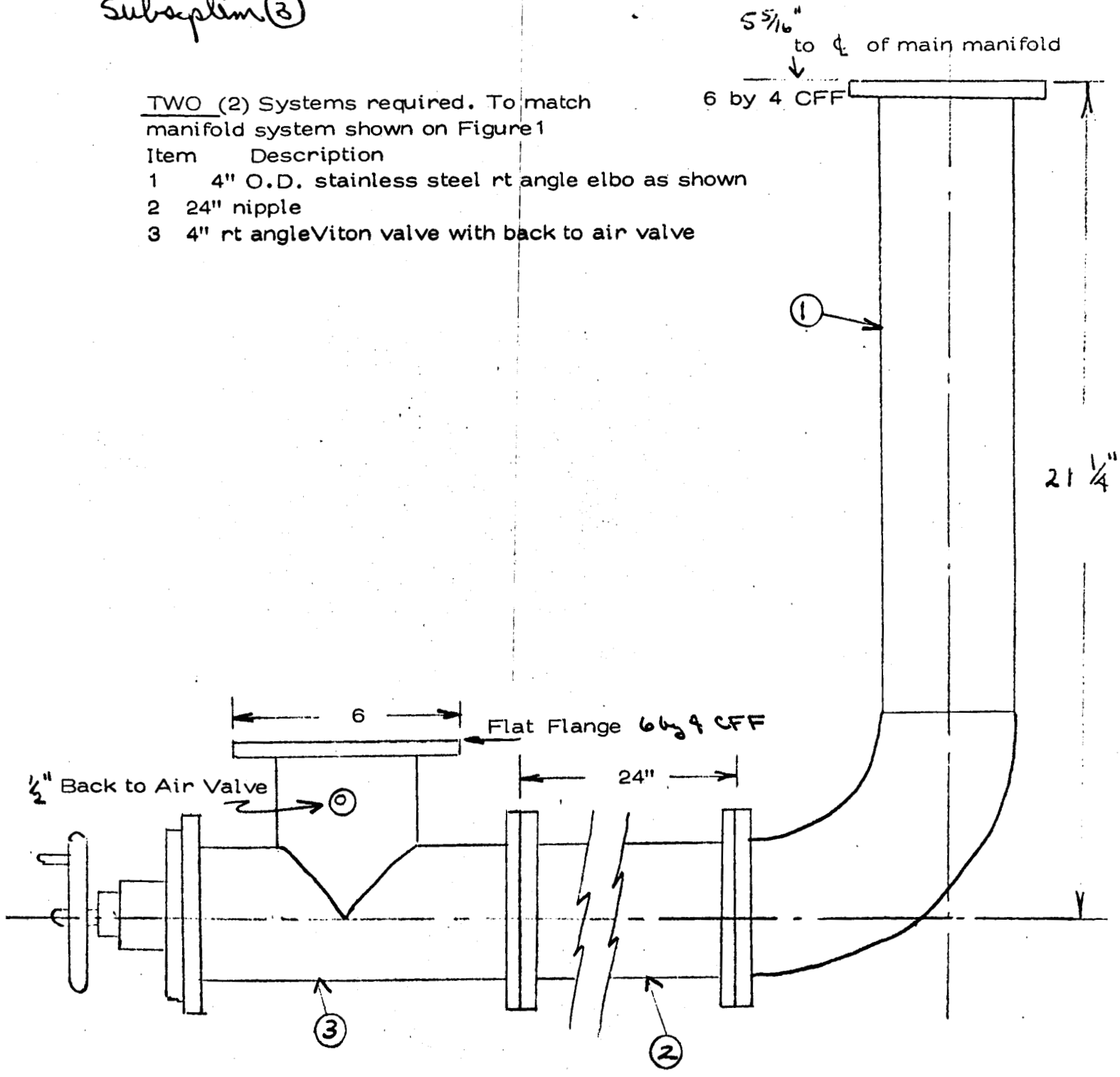

Figure I-3

Subsystem (2)

Two (2) Systems required. To match manifold system of Figure 1.

Item
1 stainless steel braided hose 1 1/2' long
2 Conflat flange with thermocouple gage and 1/2" Viton valve
3 2 1/2" Viton Rt. angle valve
4 2 1/2" O.D. nipple
5 special bypass roughing system

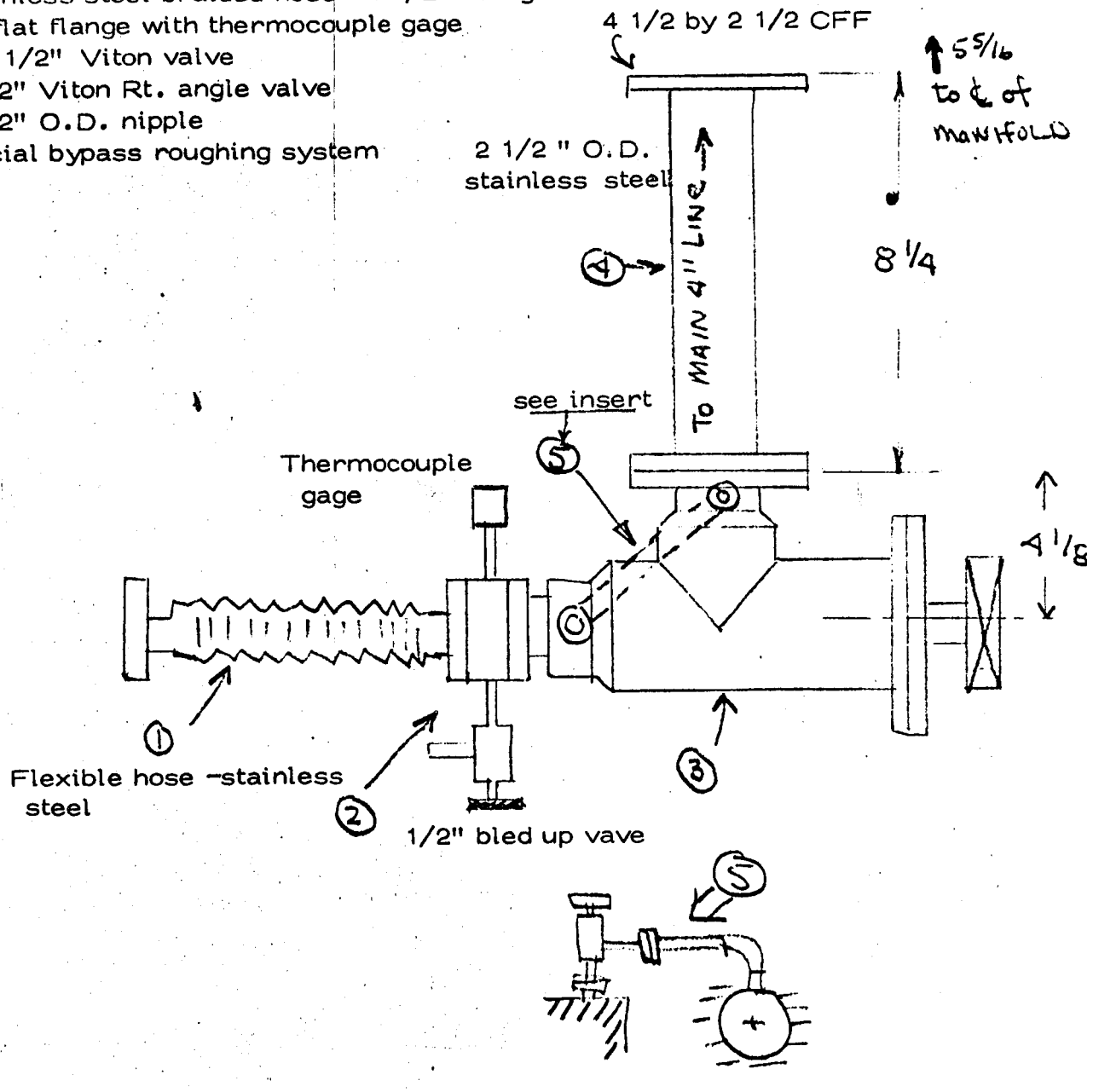

Figure I-4

Part II Thermal Radiation Studies

The modified integrating sphere reflectometer has become a standard instrument for reflectance measurements. In the use of the modified integrating sphere a sample is placed at the center of the sphere and by rotating the sample the directional reflectance can be measured [1-5]. The effects of a center-mounted sample on the sphere performance have been discussed by several authors [1,6,7]. The introduction of a center-mounted sample affects the uniformity of the sphere wall irradiance even though the sphere wall and sample surfaces are perfectly diffuse reflectors.

The present work is an experimental study of the blockage effects of a centrally located sample on the measurement of reflectance in the modified integrating sphere. The experiment was carried out for various sphere to sample radius ratios, and reflectances of front and back surface of the test sample.

Apparatus

The apparatus for these tests consisted of a modified integrating sphere reflectometer, a laser light source and an optical system, test samples, and associated detecting and recording equipment.

The integrating sphere reflectometer used was a modification of a commercially available integrating sphere radiometer (Heatransfer Laboratories, Inc., Model No. IRS-1A). The sphere was constructed of stainless steel with a 7.6 inch ID, and the inner surface was coated with a 2 to 3 mm. thick layer of magnesium oxide (MgO). Three 1.75 inch ID ports for sample, detector and light source were available.

Light from a helium-neon gas laser passed through a double convex lens which focused the light on a pinhole of 1/4 millimeter diameter. The light passing through the pinhole was made to diverge at the rate of approximately 0.01 inches per inch by a negative lens and the amount

of light entering the sphere was regulated by an iris with a maximum diameter of two inches. The iris was placed in the optical path at the point where the beam had diverged to approximately 2 inches in diameter. The laser, optical system, and integrating sphere were mounted on an optical bench, which gave rigidity to the test setup and eliminated frequent and time consuming alignments of the optical system.

The detector used was a solar cell of size 1/2 x 1 centimeter, which was attached to a rotatable arm and was located in the plane of illumination. The detector was located approximately 3/10 inches from the sphere wall with its detecting surface facing the center of the sphere and could be rotated through 360 degrees so that the sphere wall irradiance was recorded as a function of the detector position.

Test Samples

The test samples were stainless steel hemispheres of which the plane area was the sample surface and were permanently mounted on 1/8 inch diameter brass rods. The rods were coated with white paint and then given a coat of MgO. The sample port was located perpendicular to the plane of illumination and the samples could be rotated for any desired angle of illumination.

The sample surfaces were MgO over white paint over polished stainless steel; black paint (3101 Nextel Brand Suede Coating by 3M) over polished stainless steel; and polished stainless steel. The stainless steel samples were first machine and then hand polished. The thickness of MgO was approximately 1 millimeter on the white paint.

Combinations of these surfaces were also used, and samples are identified in the following way: MgO/P which means a MgO coated front surface and a polished back surface; B/MgO which means black front surface and a MgO back surface, etc.

The diameters of the test samples used were 1.5, 1.0, and 0.5 inches for the hemispheres.

Experimental Procedure

The performance of the basic sphere systems was checked for linearity of detector response and diffuseness of the sphere wall. The integrating sphere theory indicates that if light passes through an aperture into a spherical enclosure whose wall is perfectly diffuse reflecting, the irradiance on the sphere wall is uniform regardless of position. The diffuseness of the sphere wall was checked several times during the study without the center mounted sample inside the sphere. The detector arm was rotated through 360 deg. and the detector output varied less than ± 1 percent.

A test sample was placed at the center of the sphere and set for the desired angle of illumination. Then either the sample or the sphere wall was illuminated and by rotating the detector the irradiance on the sphere wall was measured as a function of detector position. A second series of measurements were made comparing detector output when the sample was fully illuminated to when the sample was displaced one diameter from the center of the sphere and the wall illuminated. In this case, the detector was located so that no first surface reflections from the sample could be detected.

Results

Diffusely Reflecting Samples, Wall Irradiance Distribution. If a perfectly diffusely reflecting plane sample is illuminated at the center of the sphere, the upper hemisphere receives more energy due to the first reflection from the sample, while the lower hemisphere does not receive any energy from the first reflection. As a result, the distribution of irra-

diance in the upper hemisphere follows closely a cosine distribution which is modified by wall reflections, while the irradiance in the lower hemisphere is almost uniform due to multiple reflections. This distribution of sphere wall irradiance has been discussed by Edwards, et. al. [1], Dawson, et.al. [6] and verified by Cho [7,8]. The results of the present study obtained with the rotatable detector along with those of Cho are shown in Fig II-1 for a system of MgO/MgO samples. Data points represent the ratio of wall irradiance at an angle, φ, from the sample normal to the wall irradiance of an empty sphere and are indicated for every 30 degrees, although the curves are drawn through data points every 10 degrees.

It can be seen in Fig II-1 that in the present study the sphere wall irradiance is for all practical purposes independent of sample size while the results of Cho and Birkebak [7] show a dependence on sample size. Cho allowed a constant amount of energy to enter the sphere and illuminate the sample. The samples were only partially illuminated, the diameter of the illuminated area being less than the diameter of the smallest sample which was 0.7 inches. Test samples of different sizes were placed in the sphere and the wall irradiance was obtained for each sample. The amount of energy reflected by the first sample reflection was the same for all of Cho's samples because the area of illumination was the same. The end result is that as the samples increased in size more area was presented for blockage and absorption, and the wall irradiance decreased as shown in Fig. II-1.

In the present study the samples were completely illuminated so that the energy per unit surface area entering the sphere was approximately the same for each sample and the samples therefore received more energy than did those of Cho. The amount of energy absorbed during the direct illumination of each sample was proportional to the sample size, but the amount of energy available for illumination and reflection was also proportional to sample size. As the samples increased in size, they presented more area for blockage and absorption, but the amount of incident energy also increased so that the wall irradiance was the same for all the samples tested as shown in Fig. II-1. The present results are 7% higher than those of Cho for $R/r = 5$,

5% higher for R/r = 7.6, and 2.5% higher for R/r = 15.2 as compared to R/r = 10 for Cho. As the sample size decreased the difference between the detected irradiance for complete and partial illumination decreases because the blockage and absorption effects decrease.

Precise calculations of wall irradiance due to a center-mounted sample requires a computer because of the many shape factors which must be obtained for each unit area. Dawson, et. al. [6], have written a computer program to do this. They consider a modified integrating sphere of radius R with a diffusely reflecting interior and the center-mounted sample is assumed to be an infinitely thin disk of radius, r. The theoretical results obtained by using this program are based on a sphere which was divided into 16 parts, and a sufficient number of reflections were considered to achieve an accuracy of 0.01 percent in the wall irradiance. The theoretical wall irradiance was calculated for the 16 spherical zones considered. The theoretical results chosen for comparison were for perfectly diffuse sample of size R/r = 5 and for reflectances of the sample, $\rho_{s_1} = 0.05$ and for the sample holder of $\rho_{s_2} = 1.00$, and for an incident angle of sample illumination of $\theta = 5.6$ degrees. The experimental results are for B/MgO sample of size R/r = 5 and the angle of incident sample illumination is $\theta = 0$ degrees. The result is shown in Fig. II-2. The experimental results are for $V_{(\varphi)}/V_{(\varphi = 90^o)}$ with the sample inside the sphere. The disagreement is due in part to the finite thickness and hemispherical shape of the test sample, and variation of ρ_{s_1} and ρ_{s_2} from the theoretical values. The increase in irradiance near $\varphi = 170$ degrees is due to sample edge effects and some direct illumination on the detector.

An analysis of the distribution of sphere wall irradiance in the upper hemisphere has been given by Edwards, et. al. [1] and Cho [8]. In their analysis the test sample is plane and perfectly diffusely reflecting. Neglecting sample size and blockage effects after the first reflection, the detector response in the upper hemisphere is:

$$V(\varphi) = \frac{kA_d E_o \rho_{s_1}}{A} \left(4\cos\varphi + \frac{\rho_w}{1-\rho_w}\right) \tag{1}$$

Normalizing equation (1) by $V(\varphi = 90^o)$, one obtains

$$\frac{V(\varphi)}{V(\varphi = 90^o)} = 1 + \frac{4(1-\rho_w)}{\rho_w} \cos\varphi \tag{2}$$

Comparison of equation (2) with the experimental data is made in Figure I-2 for a measured wall reflectance [9] of $\rho_w = 0.94$ and agreement is seen to be poor.

The extension of the center-mounted sphere theory, Appendix A, to include sample size effects is straight forward and leads to the following equation for the detector output in the upper hemisphere.

$$V(\varphi) = kA_d \rho_{s_1} e_o \left[\frac{(\frac{r}{R})^2 \cos\varphi}{\sqrt{[1+(\frac{r}{R})^2]^2 - 4(\frac{r}{R})^2 \sin^2\varphi}} + \frac{f(\frac{r}{R})\rho_w}{1-\rho_w} \right] \tag{3}$$

where

$$f(\frac{r}{R}) = \frac{1}{8} \left[(1+(\frac{r}{R})^2)^2 - \sqrt{(1+(\frac{r}{R})^2)^2 - 4(\frac{r}{R})^2}\right]$$

Representing the detector output as $V(\varphi)/V(\varphi = 90^o)$ one obtains

$$\frac{V(\varphi)}{V(\varphi = 90^o)} = 1 + \frac{(1-\rho_w)}{\rho_w} \frac{(\frac{r}{R})^2 \cos\varphi}{f(\frac{r}{R}) \sqrt{(1+(\frac{r}{R})^2)^2 - 4(\frac{r}{R})^2 \sin^2\varphi}} \tag{4}$$

Equation (4) is compared to the experimental results in Figure I-2 and good agreement is obtained. The agreement between Dawson, et.al. computer results and equation (4) is good. However, a comparison is not recommended here since the computer results are for a wall reflec-

tance of 0.96 while the experimental wall reflectance used in equation (4) is approximately 0.94.

Calculations based on equation (4) for values of (r/R) from 0.06 to 0.2 and $\varphi = 0$ results in variation of $V(\varphi)/V(\varphi = 90)$ from 1.169 to 1.162. Such a small change is difficult to measure. However, in Fig. I-1 our data shows small variations in $V(\varphi)$ which agree with the trends of equation (4). No direct comparison of equation (4) and the MgO/MgO results were made since there is some indication that the surface may have had a small specular component.

Absolute Reflectance - Sample Displacement Technique. Researchers have used several methods to obatin directional reflectance with the modified integrating sphere [1,2,4]. The method to be described here we call the displacement technique.

When a plane sample is placed at the center of a sphere and fully illuminated, the detected wall irradiance based on our second order theory gives for $\varphi > 90$ degrees,

$$V_s = k\rho_{s_1} A_d e_o f(\frac{r}{R}) [\frac{\rho_w}{1-\rho_w}] \qquad (5)$$

If the sample is displaced one diameter so that the wall is illuminated directly, the detected irradiance for $\varphi > 90$ degrees is

$$V_w = kA_d e_o f^*(\frac{r}{R})(\frac{\rho_w}{1-\rho_w}) \qquad (6)$$

where $f^*(\frac{r}{R})$ is related to the shape factor between the displaced sample and sphere wall. The result of dividing equation (5) by (6) is

$$\frac{V_s}{V_w} = \rho_{s_1} \frac{f(\frac{r}{R})}{f^*(\frac{r}{R})} \qquad (7)$$

If we assume that $f(\frac{r}{R}) \cong f^*(\frac{r}{R})$, then one obtains the "absolute" reflectance of the surface by this method. A set of tests were carried out in order to experimentally determine when one can reasonably make such an assumption. Measurements were made for the hemispherical sample holders with various combination of front and back surface reflectances. In Figure I-3 the results are present for the ratio of detector output with the sample in position to that of an empty sphere V_s/V_E. The effects of (r/R) are very evident in the results. The ratios of $V_s(r/R)/V_w(r/R)$ are within ± 1/2 percent of each other and independent of (r/R) and insensitive to small sample displacement effects. The assumption that $f(r/R) \cong f^*(r/R)$ is thus established. Similar results were found also for stainless steel and black painted test surfaces.

Discussion

In current integrating sphere practice, it is customary to neglect wall irradiance variation for the case of center-mounted samples. The assumption is usually made that blockage effects and size $(\frac{r}{R})$ effects are small and can be neglected. We have seen that for the usual range of (r/R) used in practice [0.1 to 0.15], the upper wall irradiance follows a cosine like distribution. However, when one measures reflectance by the displacement technique, the nonuniformity of sphere wall irradiance and sample size effects (r/R) are minimized.

It is the opinion of the authors that the displacement technique for reflectance measurements is preferable to the comparison method. In the comparison method the sample is placed on one side of the sample holder and a reference or standard surface on the other. By rotating the holder through 180 degrees the sample and then the reference surface can be illuminated respectively. The ratio of the detector output for this method is interpreted as the ratio of reflectances. However, if the reflectance of the sample and reference surface are greatly different, differences in sphere wall irradiance are found [6,7,8] which can cause sizeable errors in the measured reflectance. Because of this we be-

lieve that the displacement technique involves less experimental error than the comparison technique and simplicity of operation is still retained.

NOMENCLATURE

English Letters		Typical Units
A	total area of the interior sphere wall	ft^2
A_d	area of the detector	ft^2
A_s	area of the test sample	ft^2
E_o	incident energy into the sphere	Btu/hr
e_o	incident energy into the sphere	Btu/hr-ft^2
f	blockage factor	dimensionless
k	detector constant	mv/[Btu/hr]
R	radius of the sphere (= 3.8 inches)	inch
r	radius of the test sample	inch
V_E	detector response at $\varphi = 90$ degrees without sample inside sphere	mv
V_φ	detector response at φ when sample is illuminated	mv
V_s	detector response at $\varphi > 90$ degrees when sample is illuminated	mv
V_w	dtector response at $\varphi > 90$ degrees when sample is displaced	mv
Greek Letters		
ρ_{s_1}	reflectance of the front surface of the test sample	dimensionless
ρ_{s_2}	reflectance of the back surface of the test sample	dimensionless

ρ_w	reflectance of the sphere wall	dimensionless
φ	polar angle of reflection from surface normal	degrees

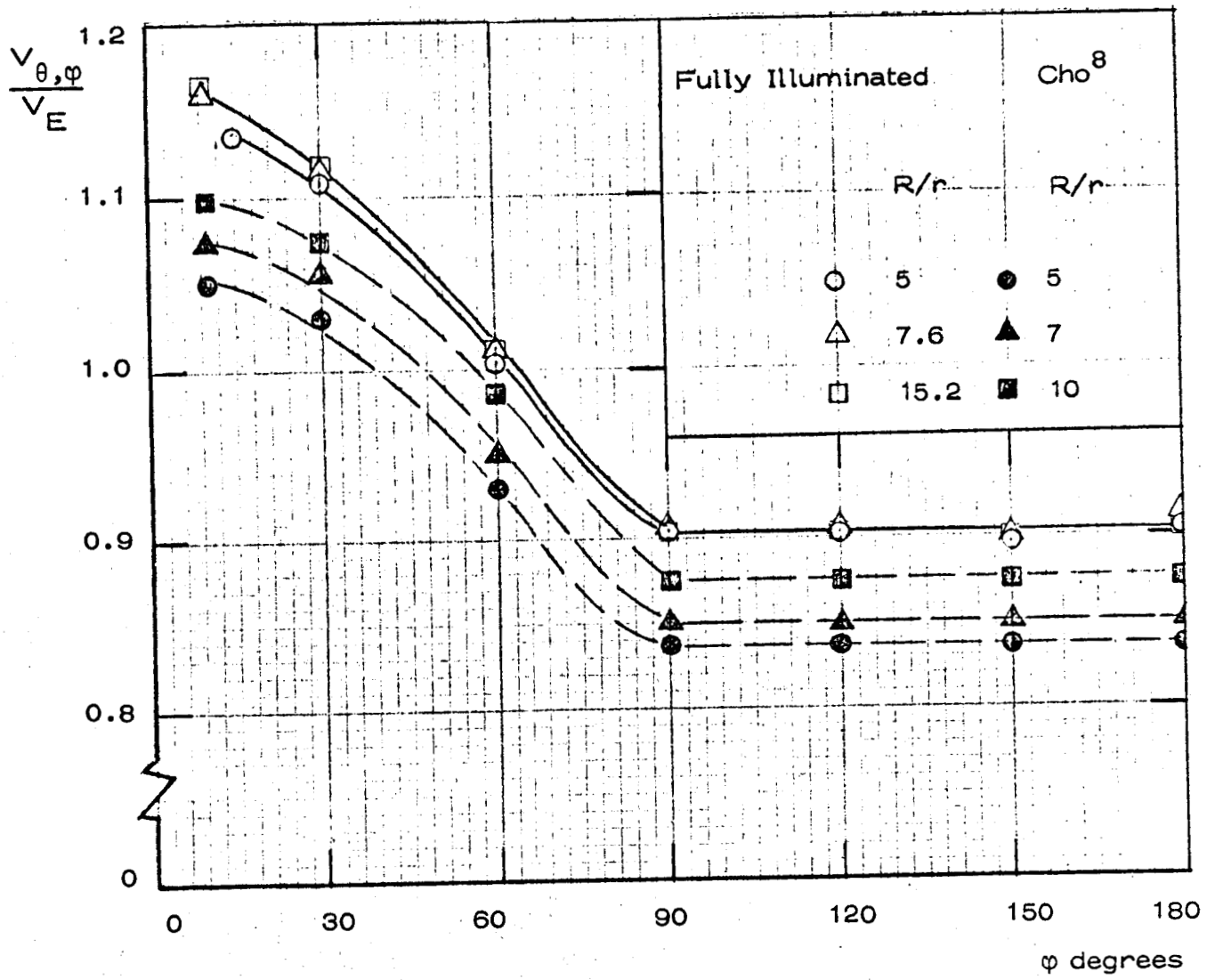

Figure II-1 Irradiance on the Sphere Wall with Plane MgO/MgO Samples

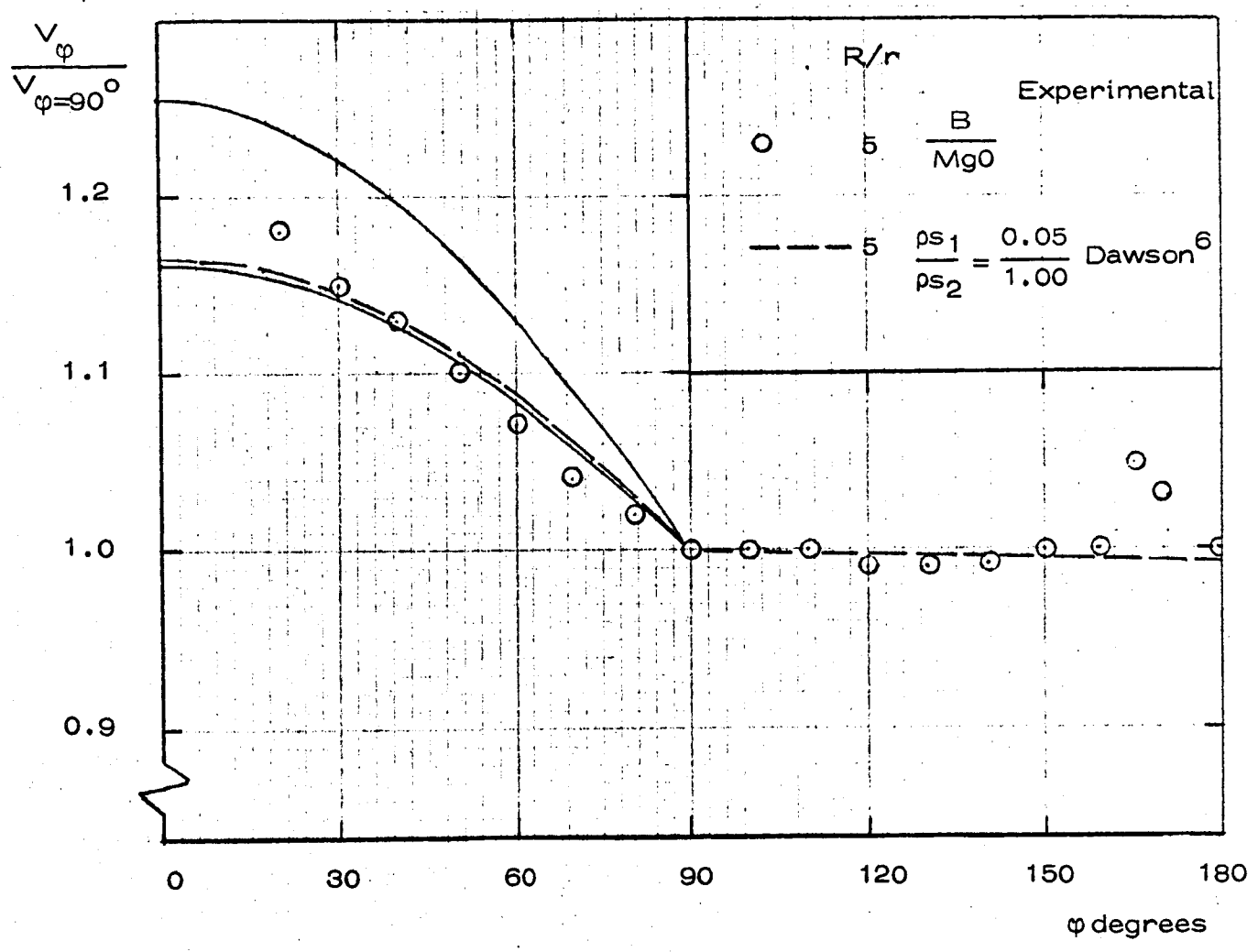

Figure II-2 Irradiance on the Sphere Wall Using A Computer Technique

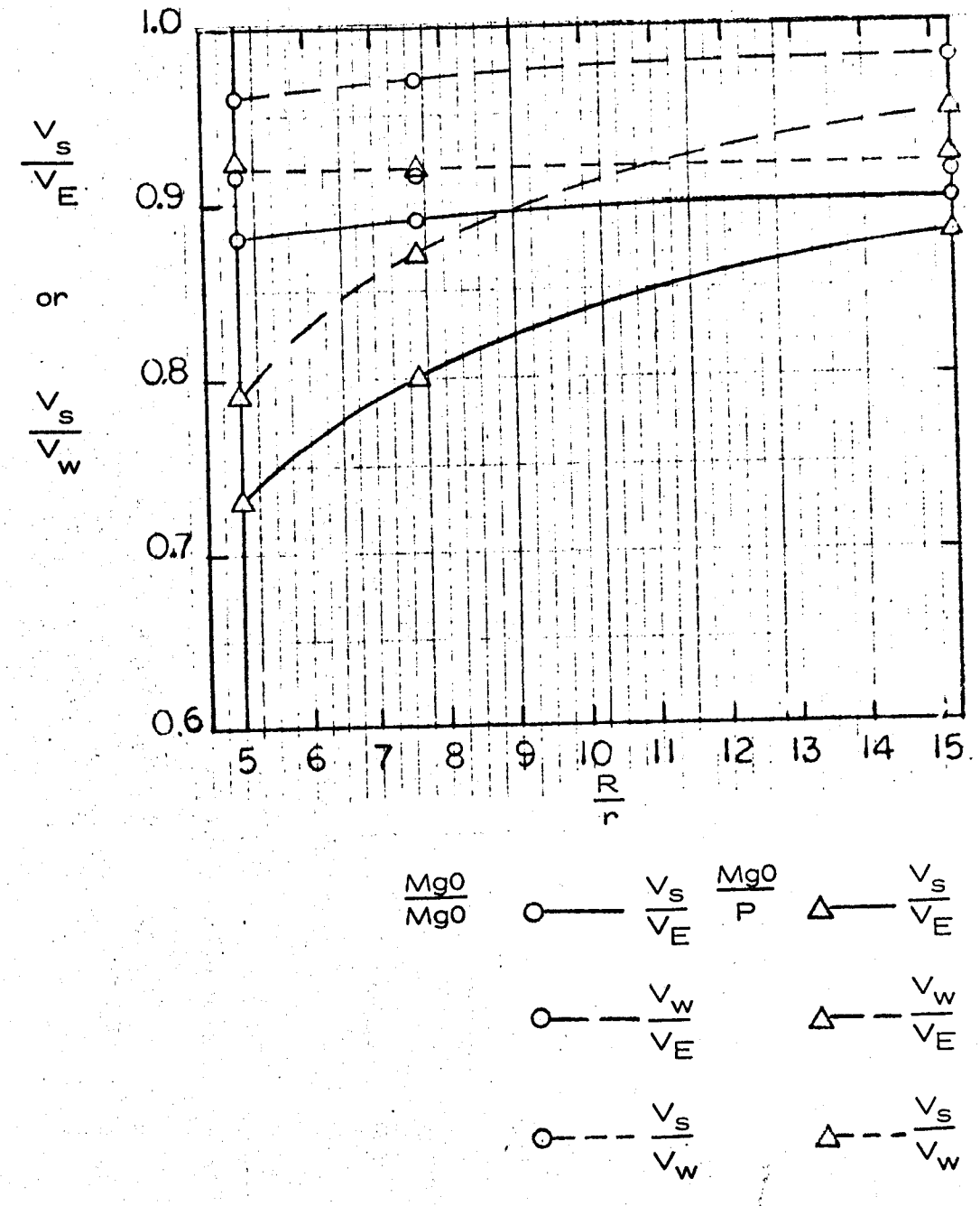

Figure II-3 Sample Blockage Effects Due to Sample Displacement

References

1. D. K. Edwards, J. T. Gier, K. E. Nelson, and R. D. Roddick, "Integrating Sphere for Imperfectly Diffuse Samples," Applied Optics, vol. 51, 1961, p. 1279.

2. W. M. Brandenberg, "The Reflectivity of Solids at Grazing Angles," NASA SP-31, Measurement of Thermal Radiation Properties of Solids, 1963, p. 75.

3. A. S. Toporets, "Study of Diffuse Reflection from Powders Under Diffuse Illumination," Optics and Spectroscopy, vol. 7, 1959, p. 471.

4. B. A. McCullough, B. E. Wood, A. M. Smith, and R. C. Birkebak, "A Vacuum Integrating Sphere for In-Situ Reflectance Measurements at 77°K from 0.5 to 10 Microns," AEDC-TR-67-10, 1967.

5. R. C. Eberhart, "Angular Dependence of Spectral Reflectance in the Infrared," M.S. Thesis, University of California, 1960.

6. J. P. Dawson, D. C. Todd, B. E. Wood, B. A. McCullough and R. C. Birkebak, "Deviations from Integrating Sphere Theory Caused by Centrally Located Samples," AEDC-TR-65-271, 1966.

7. R. C. Birkebak and S. H. Cho, "Integrating Sphere Reflectometer Center-Mounted Sample Blockage Effects," ASME Paper No. 67-HT-54, 1967.

8. S. H. Cho, "Reflectance Errors of the Modified Integrating Sphere Reflectometer," M.S. Thesis, Georgia Institute of Technology, 1966.

9. P. I. Stumbo, "Blockage Effects of Center-Mounted Samples in the Modified Integrating Sphere Reflectometer," M.S. Thesis, Department of Mechanical Engineering, University of Kentucky, January 1969.

APPENDIX II-A

Theory for the Center-Mounted Sample Integrating Sphere

The theory of the integrating sphere involves multiple reflections within a spherical enclosure. The theory presented here is for the modified integrating sphere with center mounted samples.

Let an amount of energy $[E_o = e_o A_s]$ be incident on a test sample as shown in Fig. II-4. An amount $\rho_{s_1} E_o$ is reflected into the upper hemisphere and of this energy only a fraction $dF_{A_S - dAw}$ reaches an elemental area on the wall dAw. Therefore, the energy from the sample A_S to dA_w is

$$\rho_{s_1} e_o A_s dF_{A_s - dA_w} = \rho_{s_1} e_o dA_w F_{dA_w - A_s} \tag{8}$$

where we have invoked reciprocity $A_s dF_{A_s - dA_w} = dA_w F_{dA_w - A_s}$. If a detector is located at φ on the wall, the detector output caused by irradiance on it from the samples first reflection is

$$V_1(\varphi) = k\, \rho_{s_1} e_o dA_d F_{dA_d - A_s} \tag{9}$$

The shape factor $F_{dA_d - A_s}$ can be calculated for the geometry in Fig. II-4. The result obtained is

$$F_{dA-As} = \frac{(\frac{r}{R})^2 \cos\varphi}{\sqrt{(1+(\frac{r}{R})^2)^2 - 4(\frac{r}{R})^2 \sin^2\varphi}} \tag{10}$$

The energy reflected from the sample to the wall, equation (8), is reflected by the wall, of this the following amount is incident on the detector dA_d at φ from first wall reflection.

$$\rho_w[\rho_{s_1} e_o dA_w F_{dA_w - A_s}] dF_{dA_w - dA_d} \tag{11}$$

Summary over the dA_w's [upper hemisphere] that contribute to the detector output for these reflections one gets

$$V_2(\varphi) = k\int_0^{2\pi}\int_0^{\pi/2} \rho_w \rho_{s_1} e_o dA_w F_{dA_w - A_s} dF_{dA_w - dA_d} \tag{12}$$

The shape factor $d\,F_{dA_w - dA_d}$ in the spherical enclosure is

$$dF_{dA_w - dA_d} = \frac{dA_d}{Aw} \tag{13}$$

Therefore, using equations (10) and (13) one gets

$$V_2(\varphi) = k\int_0^{2\pi}\int_0^{\pi/2} \frac{\rho_w \rho_{s_1} e_o dA_d (\frac{r}{R})^2 \cos\varphi'\, R^2 \sin\varphi' d\varphi' d\theta}{A_w \sqrt{(1+(\frac{r}{R})^2)^2 - (2\frac{r}{R})^2 \sin^2\varphi'}} \tag{14}$$

where $dA_w = R^2 \sin\varphi' d\varphi' d\theta$ and $A_w = 4\pi R^2$. The double integral can be evaluated over the upper hemisphere and one obtains

$$V_2(\varphi) = \frac{k}{8} \rho_w \rho_{s_1} e_o dA_d [(1+(\frac{r}{R})^2 - \sqrt{(1+(\frac{r}{R})^2)^2 - 4(\frac{r}{R})^2}] \tag{15}$$

We now consider the irradiance on an area dA_w in the upper hemisphere for first reflections from the wall. The formulation is similar to equation (11), that is

$$\rho_w[\rho_{s_1} e_o dA_w F_{dA_w - A_s}] dF_{dA_w - dA_w'} \tag{16}$$

and the total amount of irradiance received by dA_w' in the upper hemisphere is

$$\rho_w \rho_{s_1} e_o dA'_w f(\frac{r}{R}) \tag{17}$$

where $f(\frac{r}{R}) = \frac{1}{8}\left[[1+(\frac{r}{R})^2]^2 - \sqrt{(1+(\frac{r}{R})^2 - 4(\frac{r}{R})^2}\right]$

Next, in order to simplify the calculations, we assume that we can neglect sample blockage effects after first reflections from the sample. Therefore, equation (17) is valid for all dA_w's on the sphere. This assumption is justified when we consider the shape factors of a differential area dA_w with respect to the sample A_s and sphere wall A_w. For the largest sample to sphere radius ratio considered in this report, from equation (10) with $r/R = 0.2$, $F_{dA_w - A_s} \cong 0.04$ for $\varphi = 0^o$, when φ goes to 90°, $F_{dA_w - A_s} = 0$. The shape factor of the whole upper hemisphere to a sample when $(r/R) = 0.2$ is 0.1. Therefore, it seems reasonable to assume that after the initial sample reflection that the effect of the center-mounted sample are small and can be neglected for a first approximation to the more exact theory.

We now apply this line of thought to the remaining infinite number of wall reflections. The amount of radiation detected after two wall reflections is

$$V_3(\varphi) = k\int_{A_w} \rho_w^2 \rho_{s_1} e_o f(\frac{r}{R}) dA_d \frac{dA'_w}{Aw} = k\rho_w^2 \rho_{s_1} e_o f(\frac{r}{R}) dA_d \tag{18}$$

for subsequent reflections

$$V_4(\varphi) = k\rho_w^3 \rho_{s_1} e_o f(\frac{r}{R}) dA_d$$

$$- - - - - - - - - - - -$$

$$- - - - - - - - - - - - \qquad (19)$$

$$- - - - - - - - - - - -$$

$$V_n(\varphi) = k\rho_w^n \rho_{s_1} e_o f(\frac{r}{R}) dA_d$$

The total detected irradiance for a detector in the upper hemisphere is

$$V(\varphi) = kA_d \rho_{s_1} e_o \left[\frac{(\frac{r}{R})^2 \cos\varphi}{\sqrt{(1+(\frac{r}{R})^2)^2 - 4(\frac{r}{R})^2 \sin\varphi}} + \frac{f(\frac{r}{R})\rho_w}{1-\rho_w} \right] \qquad (20)$$

where we have replaced dA_d with A_d.

When the detector is in the lower hemisphere ($90^o \leq \varphi \leq 180^o$), the first reflection from the sample is not detected, $V_1 = 0$. The detector response for the second, third, etc. reflections are identical to those previously calculated. Therefore, the total detector response in the lower hemisphere is

$$V = k\rho_{s_1} e_o A_d f(\frac{r}{R}) [\frac{\rho_w}{1-\rho w}] \qquad (21)$$

For a detector at $\varphi = 90$ both equations (20) and (21) give the same result which is the expected result.

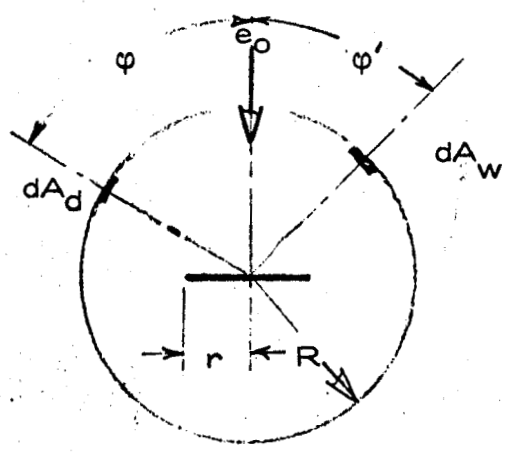

Figure II - 4

Coordinate System

Part III Thermal Conductivity Measurements

A number of test cells have been constructed which are meant to provide backup measurements for the proposed conductivity measurements. The proposed measurements require the sensing of the monochromatic radiation intensity from a free surface of the lunar material. Since the moon temperatures are low, laboratory radiation measurements at these temperatures require an infrared spectrometer capable of sensing radiations with wavelengths out to 50 μ. The thermal conductivity has never before been obtained by such a measurement technique and the possibility exists that unforeseen problems may arise which will lead to inaccurate measurements. For this reason standard methods are being employed at first to make measurements of the thermal conductivity of known materials. These conductivities are being compared with those measured by other investigators. Later, when the infrared spectrometer is set up, the new method will be checked out using the same materials. The results from all methods should agree.

In addition, a thermal conductivity cell for use at higher temperatures with the radiation technique has been constructed for use in a separate vacuum chamber. This cell can be used with less sensitive radiation detectors.

Guarded Plate Apparatus

A schematic view of this apparatus is shown in Figure III-1. This is a standard device [1] which uses Fourier's law describing steady state heat conduction in a one dimensional homogeneous medium. That is

$$Q = -kA\frac{dT}{dx} = -kA\frac{(T_B - T_s)}{\Delta x} \tag{22}$$

If the conductivity is assumed constant, then a measurement of the total heat flux Q, the area A normal to the heat flow, and the temperature drop across the specimen will yield the conductivity. Guard heaters are provided on the bottom and sides so that there is zero temperature drop across these walls. Consequently, all heat generated in the main heater flows out through the specimen and is carried away by the water calorimeter. The calorimeter was designed as a backup device for measuring the heat flow. However, it proved to be inaccurate and inconsistent in results obtained from it. It is felt that this is due to the small differential temperatures which had to be measured plus the low flow rates of coolant through the calorimeter.

The results of measurements on powdered basalt are given in Table III-1 along with the results of two other investigators. Note that there is fair agreement.

Line Heat Source

Two cells and one probe have been built using the principle of the line heat source [2]. For an infinitely long constant line heat source, it can be shown that the temperature rise in the surrounding medium at a time t after heating begins is given by

$$\theta = -\frac{q}{4\pi k} Ei\left(\frac{-r^2}{4\alpha t}\right) \tag{23}$$

where θ is the temperature above the initial temperature at a distance r from the source, q is the heat generation per unit length of the source,

α is the thermal diffusivity and k is the thermal conductivity. It is possible to express the exponential integral with a series [3] so that

$$\theta = \frac{q}{4\pi k}\left[-\gamma - \ln z + z - \frac{z^2}{2.2!} + \frac{z^3}{3.3!} + \cdot\cdot\right] \tag{24}$$

where

$$z = \frac{r^2}{4\alpha t}$$

Then in the limit of large time, $z \ll -\ln z$ and we can write for the temperature change with time at a given r,

$$\theta_1 - \theta_2 = \frac{q}{4\pi k} \ln \frac{t_1}{t_2} \tag{25}$$

This is the working equation for the line heat source method. A measurement of the time temperature history at some point in the medium, along with a measurement of the heat input yields the thermal conductivity. The θ versus ln t plot (e.g., Figure III-2) is usually "S" shaped with the straight line portion in the center being used for the conductivity measurements. The curved portion at low time is due to the finite heat capacity of the probe while the curved portion at large time is due to axial conduction. A complete discussion of the errors incurred with such a probe is given by Blackwell and others [3,4,5].

One of the line heat source thermal conductivity cells is shown in Figure III-3 and data for glass beads taken in this cell are given in Table III-1. The data presented are averages of several measurements in each case. The heater wire is 30 ga. Nichrome and is heated electrically. The thermocouple close to the heater wire was used as the probe to measure the temperatures in equation (25) while the other couple was used to indicate the length of time it took the heat to reach the region near the cell

wall. This was found to be about five minutes. It was felt that data taken after this time might be inconsistent since the heater wire would no longer see an "infinite" medium. It appears that the hump in the data of Figure III-2 near ln t = 6.4 is due to just such an effect. Note that times as short as 90 seconds or so can be used to get meaningful results. When this was discovered it was decided to build a considerably smaller cell so that it would be possible to have a backup method for use with a small quantity of lunar surface material in case the primary method failed. The possibility also is offered that such a line heat source probe be built into the radiation cell for the lunar material. This would be highly desirable since it would provide an entirely independent method of conductivity determination in the same cell.

The second cell is shown in Figure III-4. A thermocouple is used for temperature measurement in this cell at present. Later, the heater wire will be calibrated as a resistance thermometer so that the simple circuit also shown in Figure III-4 can be used for all the data. A Honeywell 620 digital data acquisition system with an input inpedance of about 10^7 ohms is being used to record the three significant voltages. The setup at present records voltage up to 750 vdc and down to 1 μ vdc with four place accuracy. With the present setup it should be possible to record the wire temperature as a function of time to well within a degree and to measure the heat input to about ± 1%. At present there are some problems in putting the system channel scanner and printer into operation and so the method has not yet been tried. With this cell we have measured the conductivity of a 5 gram sample of powdered basalt (Table III-1).

A line heat source probe for direct insertion into a test medium is shown in Figure III-5. The probe consists of a heater wire wrapped around a hollow porcelain tube which has a thermocouple at the center. This type of probe is in common use for conductivity measurements in

soils. Data taken with this probe were not consistent with other measurements. The reason for this is probably due to the requirement of a specimen of large volume for this relatively large thermal capacity probe. The probe has subsequently burned out and will not be replaced, at least in the near future.

Radiation Cell

The first model of the radiation cell is designed to be used at relatively high temperatures on the order of 400°K along with a near infrared spectrometer. Schematically it looks the same as the guarded plate apparatus shown in Figure III-1 except that the upper surface temperature measurement is replaced by a monochromatic radiation intensity measurement. A heater winding in the base provides a known heat flux Q through the specimen of thickness Δx. Guard heaters are provided on the bottom and sides to constrain the primary heat flow in the desired path. A thermocouple in the base of the specimen cell provides a base temperature T_B. The unmeasured surface temperature is T_S. If two slightly different heat fluxes Q_1 and Q_2 are employed in two different runs, then Fourier's law gives

$$Q_1 = KA \frac{(T_{B1} - T_{S1})}{\Delta x} , \quad Q_2 = - KA \frac{(T_{B2} - T_{S2})}{\Delta x} \tag{26}$$

Additionally the center of the exposed specimen surface is focused on the slit of a spectrometer with the wavelength set near the wavelength of maximum intensity for the temperatures used. Then the ratio of Planck's law written for the two conditions is

$$\frac{i_{\lambda 1}}{i_{\lambda 2}} = \frac{(e^{C_2/\lambda T_{S_2}} - 1)}{(e^{C_2/\lambda T_{S_1}} - 1)} \frac{\epsilon_{\lambda 1}}{\epsilon_{\lambda 2}} \tag{27}$$

where C_2 is a constant. The two heating conditions will be as similar as possible concomitant with an accurate measurement of $i_{\lambda 1}/i_{\lambda 2}$. Then for the small (say 50°) surface temperature difference, $\epsilon_{\lambda 1} \cong \epsilon_{\lambda 2}$, then there remain three equations in three unknowns: T_{S1}, T_{S2}, and k and therefore k can be obtained as a function of temperature. No data has yet been taken with this probe.

Table III-1 Data Taken on Simulated Lunar Specimens

Material	Thermal Conductivity (watt/meter - ^{o}K)			
	present experiment	method	other investigators	(ref.)
Powdered basalt	0.134	(s)	0.10	(7)
	0.123	(g)	0.19	(8)
Glass beads	0.174	(s)	0.15	(7)
	0.188	(p)	0.19	(9)
	0.151	(l)		

s small line heat source

l large line heat source

g guarded flat plate

p line heat source probe

References

1. M. Jakob, Heat Transfer, vol. 1, Wiley, 1948.

2. H. S. Carslaw, J. C. Jaeger, Conduction of Heat in Solids, Oxford, 1959.

3. M. Abramowitz, I. A. Stegun, Handbook of Mathematical Functions, AMS 55, National Bureau of Standards, 1964.

4. H. J. Blackwell, "The Axial-Flow Error in the Thermal Conductivity Probe," Canadian J. Phys., vol. 34, 1956.

5. H. J. Blackwell, "Radial-Axial Heat Flow in Regions Bounded Internally by Circular Cylinders," Canadian J. Phys. vol. 31, 1953.

6. A. E. Wechsler, M. A. Kritz, "Development and Use of Thermal Conductivity Probes for Soils and Insulations," Proceedings of the Fifth Thermal Conductivity Conference, J. D. Plunkett, e., University of Denver, 1966.

7. A. E. Wechsler, P. E. Glaser, "Thermal Conductivity of Non-Metallic Materials," Summary Report to NASA under contract NAS 8-1567, June 1964.

8. E. C. Bernett, H. L. Wood, L. D. Jaffee, H. E. Martens, "Thermal Properties of a Simulated Lunar Material in Air and Vacuum," AIAA J., 1, p. 1402, 1963.

9. S. Massamune, J. M. Smith, "Thermal Conductivity of Beds of Spherical Particles," Ind. & Eng. Chem., Fundamentals, 2, p. 136, 1963.

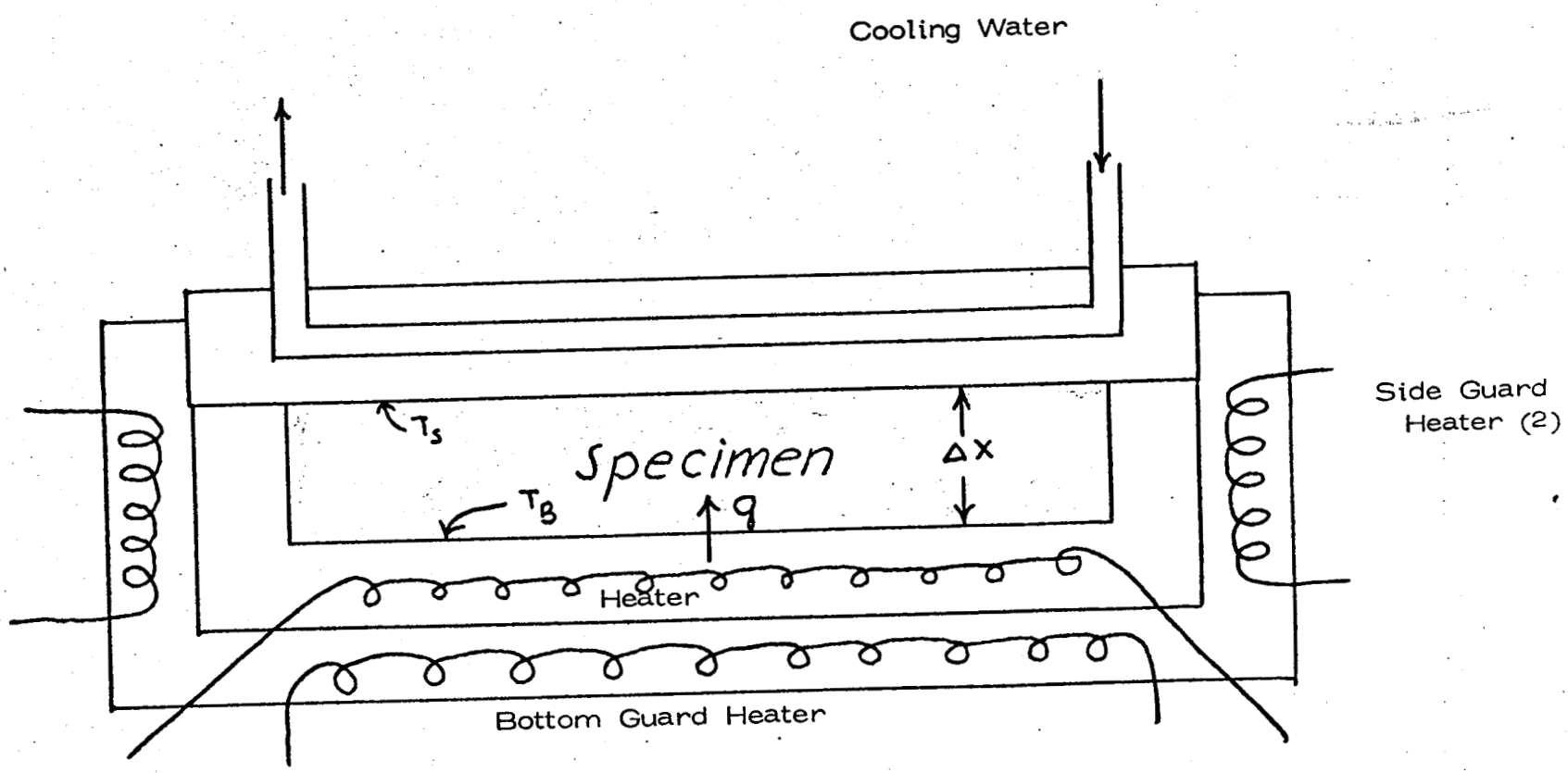

Figure III-1 Schematic View of Guarded Plate Apparatus

10 X 10 TO THE CM. 359-14
KEUFFEL & ESSER CO.

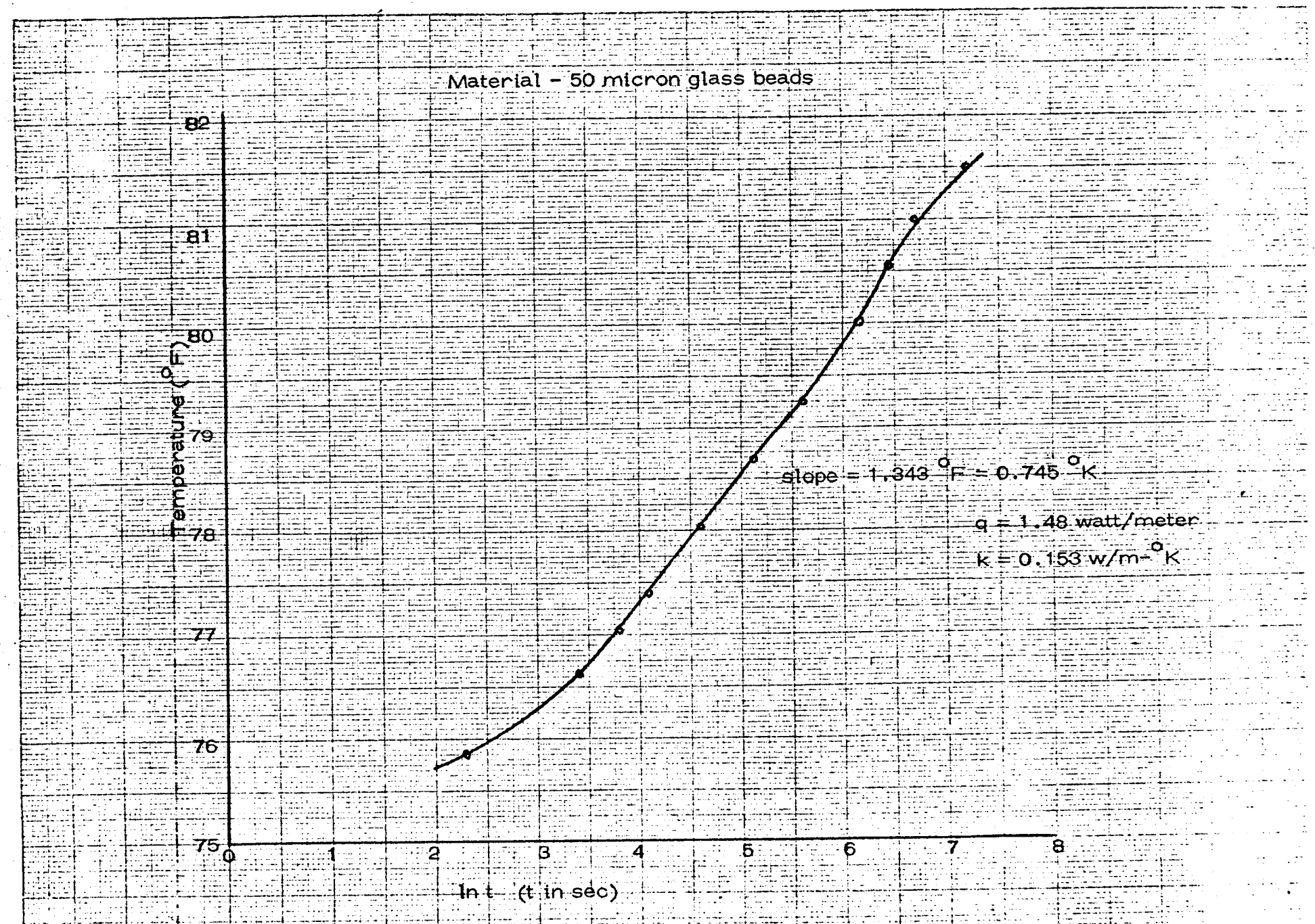

Figure III-2 — Data from Typical Line Heat Source Run

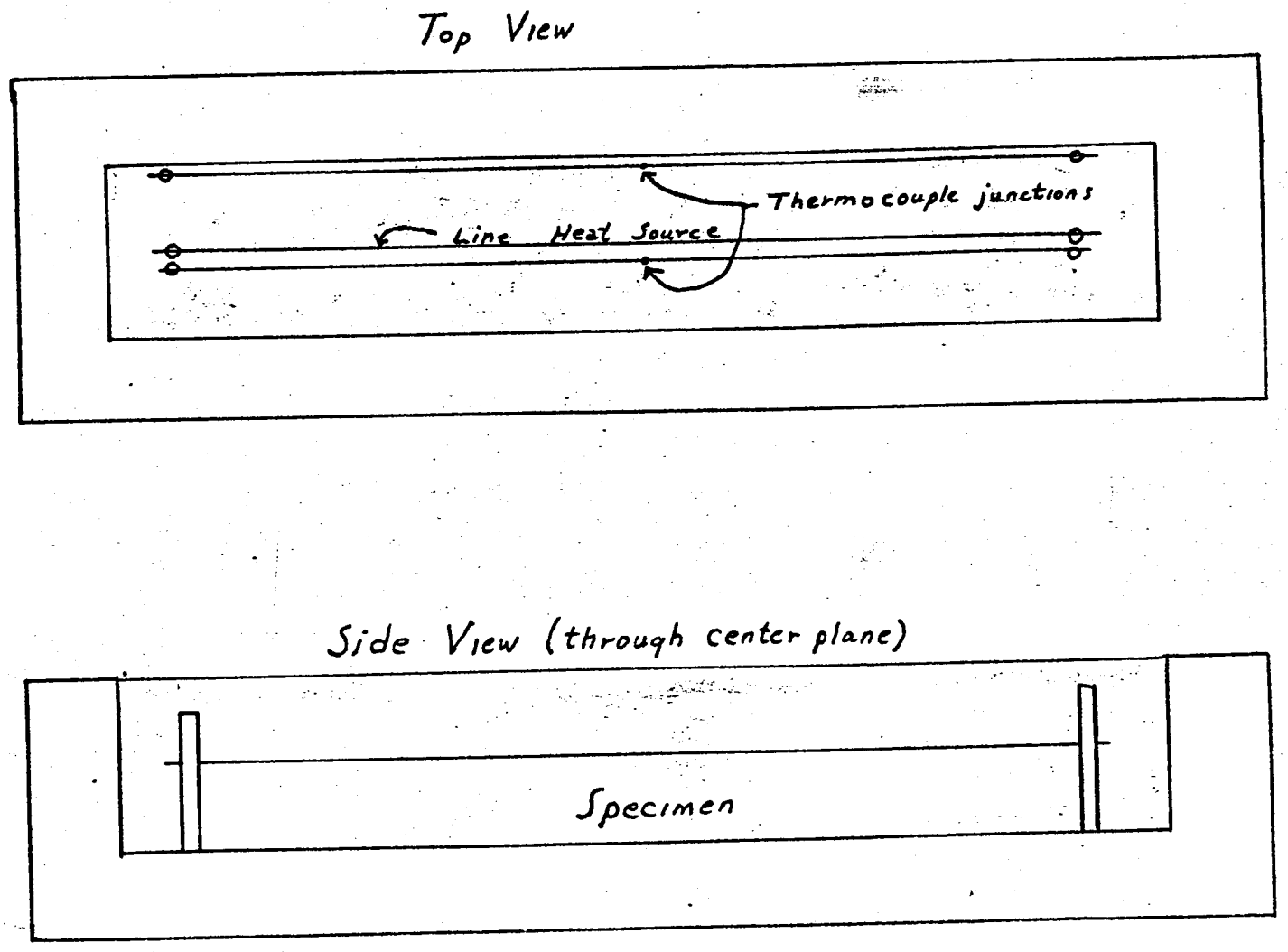

Figure III-3 Schematic View of Large Line Heat Source Probe (Approximate Size)

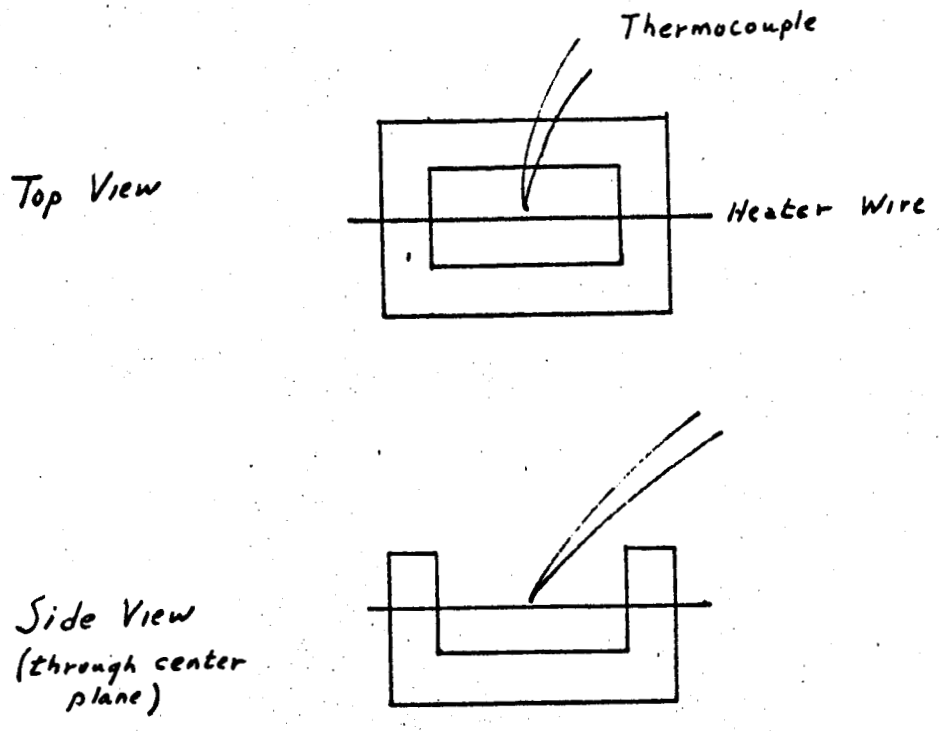

(Approximate Size)

Figure III-4 Schematic View of Small Line Heat Source Cell

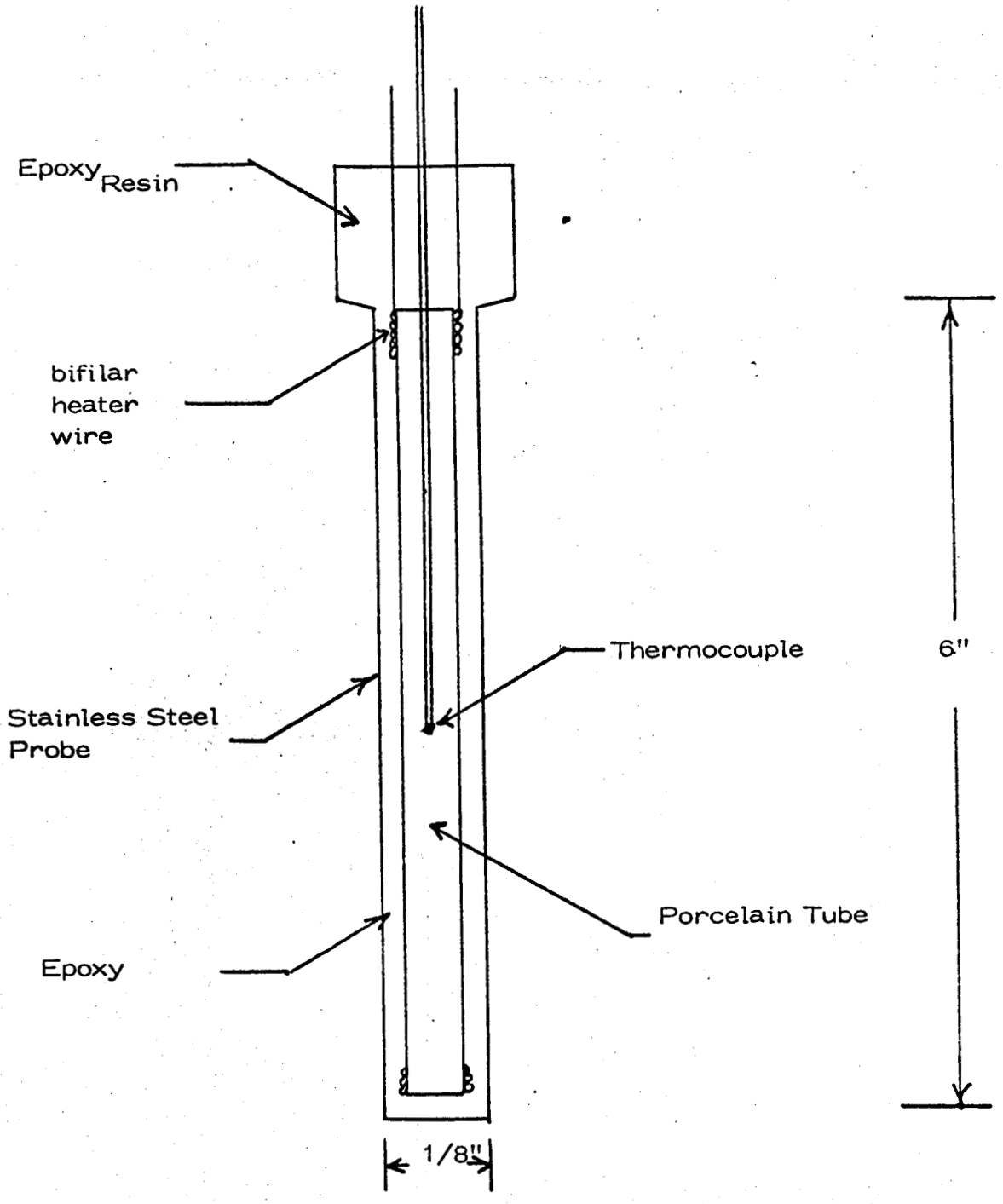

Figure III-5 Schematic View of Line Heat Source Probe